THE JOURNAL OF PHYSICAL CHEMISTRY LETTERS
A JOURNAL OF THE AMERICAN CHEMICAL SOCIETY

pubs.acs.org/JPCL Letter

Dissociation and Reformation of CO_2 Clathrate Hydrate Cages in Amorphous Ice Thin Film under Ultrahigh Vacuum

Bijesh K. Malla, Soham Chowdhury, Gaurav Vishwakarma, Rajnish Kumar,* and Thalappil Pradeep*

Cite This: J. Phys. Chem. Lett. 2025, 16, 4982−4989 Read Online

ACCESS | Metrics & More | Article Recommendations | Supporting Information

ABSTRACT: The formation of clathrate hydrates (CHs) within amorphous ice holds significant astrochemical importance. CO_2 typically forms structure I (sI) CH under vacuum, upon nucleation from an amorphous water-CO_2 ice mixture. This study presents the first report of structure II (sII) CO_2 CH, where CO_2 occupies large cages in the presence of dimethyl ether (DME) or tetrahydrofuran (THF) under ultrahigh vacuum (UHV) conditions. Mixed CHs of DME-CO_2 were prepared by sequential vapor phase deposition of CO_2:water mixture over DME at 10 K and thermally annealing this mixed ice film to 130 K. During the formation of large cages of sII CH of DME, partial dissociation of the preformed small cage of sI of CO_2 CH occurs along with the formation of new large cages of sII CO_2 CH. Similar results were observed for THF-CO_2 mixed CHs. Additionally, mixed CHs of THF-DME-CO_2 formed sII hydrates when annealed at 130 K. Prolonged annealing (37 h) at 130 K led to the dissociation of mixed CHs, releasing CO_2 and DME and increasing the THF CH fraction. These observations highlight the greater stability of THF CH compared with those of CO_2 and DME under identical conditions. These findings enhance our understanding of the structural dynamics and formation mechanisms of mixed CHs under simulated interstellar conditions.

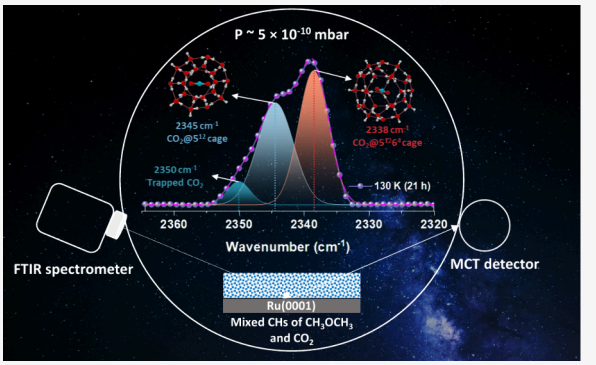

Formation of clathrate hydrates (CHs) under laboratory interstellar conditions of temperature (~10−100 K) and pressure (~10^{-10} mbar) is now well-known,[1,2] and these studies have been performed mostly with two components (a hydrate-forming guest molecule and water).[3−6] Although the original report used reflection absorption infrared spectroscopy (RAIRS),[2] the formation has also been confirmed recently by reflection high energy electron diffraction (RHEED).[7] The CHs manifest as host−guest complexes, with water molecules as the host, generating diverse cage structures to encage guest molecules such as CH_4, C_2H_6, C_3H_8, CO_2, N_2, and O_2, among others.[8−10] They typically exhibit three distinct crystalline structures, known as structure I (sI, cubic $Pm\bar{3}n$), structure II (sII, cubic $Fd\bar{3}m$), and structure H (sH, hexagonal $P6/mmm$).[11,12] These CHs were previously thought to form only under high-pressure circumstances.[13,14] Blake et al.'s study in 1991 demonstrated that CO_2 CH can form under high vacuum (10^{-6}−10^{-7} Torr) conditions too, using infrared spectroscopy and selected area electron diffraction.[15] The period of 1900−2000 witnessed extensive investigations in vacuum in the range of 10^{-6} to 10^{-8} Torr and temperatures near 80 to 150 K.[16−21] Ghosh et al. showed that CH_4 and CO_2 CH form even at 30 and 10 K, respectively, under ultrahigh vacuum (UHV, 5 × 10^{-10} mbar) conditions, where condensed molecules desorb at much lower temperatures than in high vacuum (~10^{-6} Torr).[2] There were questions that arose regarding the formation of these hydrates in unusual thermodynamic conditions, as highlighted by Choukroun et al.,[22] and they were addressed by Ghosh et al.[23] Subsequent investigations explored various CHs within UHV under cryogenic conditions.[5,6,24,25] The existence of CHs in UHV has also been shown by electron diffraction, as mentioned earlier.[7] A recent study has also demonstrated the possibility of formation of CO_2 CH at 10 K under UHV.[1] More than 300 atomic, ionic, and molecular species have been detected to date in the interstellar medium (ISM). Under such conditions, these molecules exist in the solid state or in the gas phase.[26] These condensed molecular matrices hold a wide spectrum of molecules together with water, which raises the possibility of formation of mixed and complex CHs.[27]

Typically, CO_2 and such small molecules usually form stable sI CH with 100% occupancy of the large $5^{12}6^2$ cages, and up to 70% occupancy of the small 5^{12} cages, under high-pressure conditions.[28−34] Additionally, the formation of sI CH of CO_2 has also been observed under cryogenic conditions in high vacuum.[1,2,24,35] In the presence of larger guest molecules such

Received: February 7, 2025
Revised: May 6, 2025
Accepted: May 7, 2025
Published: May 12, 2025

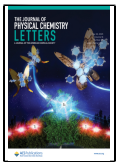

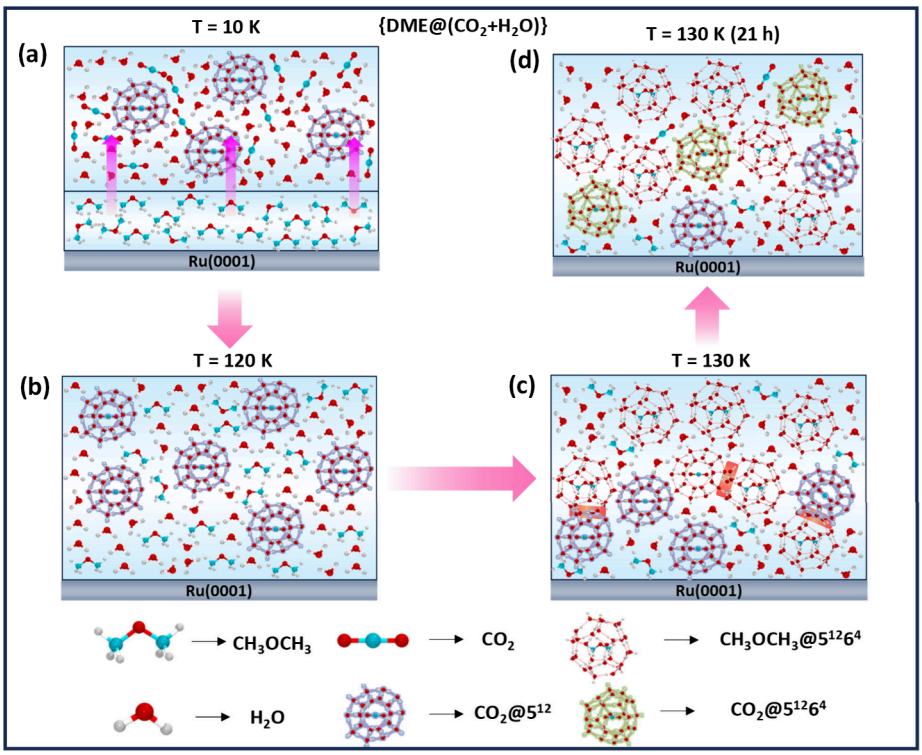

Figure 1. Schematic diagram for the reconstruction of large cages of sII CO_2 CH in the presence of DME molecules. The sequence involves the stepwise deposition of 150 ML of DME followed by 150 ML of a CO_2 + H_2O (1:10) ice mixture under conditions of 10 K (a), followed by thermal annealing to 120 K (b), 130 K (c), and a subsequent state after 21 h at 130 K (d). Small red rectangles in panel c demonstrate the interaction of large cages ($5^{12}6^4$) of DME with small cages (5^{12}) of CO_2.

as THF and cyclopentane, CO_2 mixed hydrates form classical sII CHs, where the larger guest molecules occupy the large $5^{12}6^4$ cages, and CO_2 occupies the small cages of sII, in both high-pressure and vacuum conditions.[21,36,37] Under high-pressure conditions, CO_2 can exist in $5^{12}6^4$ cages in presense of 1,3-dioxolane.[38,39] However, there is no report of its occupancy in large cages of sII mixed hydrates in UHV, with larger guest molecules capable of forming sII CHs. Additionally, the formation of mixed CHs of CO_2 with various guest molecules under UHV remains unexplored.

In this work, we have carried out an experiment taking two large guest molecules, DME and THF, separately, along with CO_2, in the form of an amorphous solid at 10 K, and subjected the mixture to anneal at 130 K. Both DME and THF have good solubility in water, and individually they are known to form classical sII hydrates in high-pressure as well as UHV conditions.[25,40−43] While CO_2[44] and DME[45] are confirmed constituents of the ISM, THF is yet to be detected there. The identification of structurally related ethers such as propylene oxide[46] and ethylene oxide,[47] however, suggests that THF could become observable with continued advancements in astrochemical detection techniques. In this work, we have studied the structural transition of CO_2 CH, when the CO_2+water mixture is sequentially deposited with THF or DME (abbreviated to THF/DME subsequently). It was observed that in the presence of THF/DME upon annealing, CO_2 moves from the small cages (in sI) and helps nucleate the sII hydrate, where it also occupies the large cages along with THF/DME. During this study, the formation of mixed CHs of CO_2, DME, and THF was also observed when both the large guest molecules were sequentially deposited along with CO_2 and water. All the experiments were carried out using a custom-built UHV instrument,[48,49] described in the Supporting Information (SI). Details of the experimental protocols and sample preparation are also presented in the SI.

The first set of experiments were performed with codeposited CO_2 and water vapor at a ratio of 1:10, on a Ru(0001) substrate, subsequently annealed to 120 K, and we observed the same results as reported previously.[2] In Figure S1, at 10 K, the two peaks at 2354 and 2346 cm^{-1} represent the pure CO_2 clusters in amorphous ice and CO_2 occupying the small cages of sI CH, respectively.[14] Typically, pure 100 ML of CO_2 ice at 10 K shows a RAIRS peak at 2381 cm^{-1} due to the LO mode of the C=O antisymmetric stretching region, where lowering the thickness leads to the redshift.[24,50,51]

The peak at 2346 cm^{-1}, however, arises from CO_2 interacting with or being trapped within the H_2O ice matrix, without contributions from LO or transverse optical (TO) coupling.[51] According to literature,[3,15,17,21,52] the 2346 cm^{-1} peak is assigned to the small cages of sI clathrate hydrates, although there was a debate regarding this assignment.[22] In our study, the 2346 cm^{-1} feature is attributed to the small cage of the sI CH of CO_2. This is in agreement with the fact that after 120 K, only one peak at 2346 cm^{-1} is seen. We then annealed the same mixture at 130 K for 6 h and observed a 2 cm^{-1} peak shift to 2344 cm^{-1} and a decrease in the peak intensity, which were attributed to partial dissociation of the small cage of sI, followed by desorption of CO_2 from the ice matrix. This suggests the metastable nature of sI CH of CO_2 at 130 K. It is noteworthy that our RAIR resolution is 2 cm^{-1}, a factor that is important for the observed peak position.

Subsequently, mixed CHs of DME and CO_2 were created by thermally annealing DME, water, and CO_2 ice mixtures at 130 K for tens of hours (Figure 1). First, 150 ML of DME vapor

https://doi.org/10.1021/acs.jpclett.5c00393
J. Phys. Chem. Lett. 2025, 16, 4982−4989

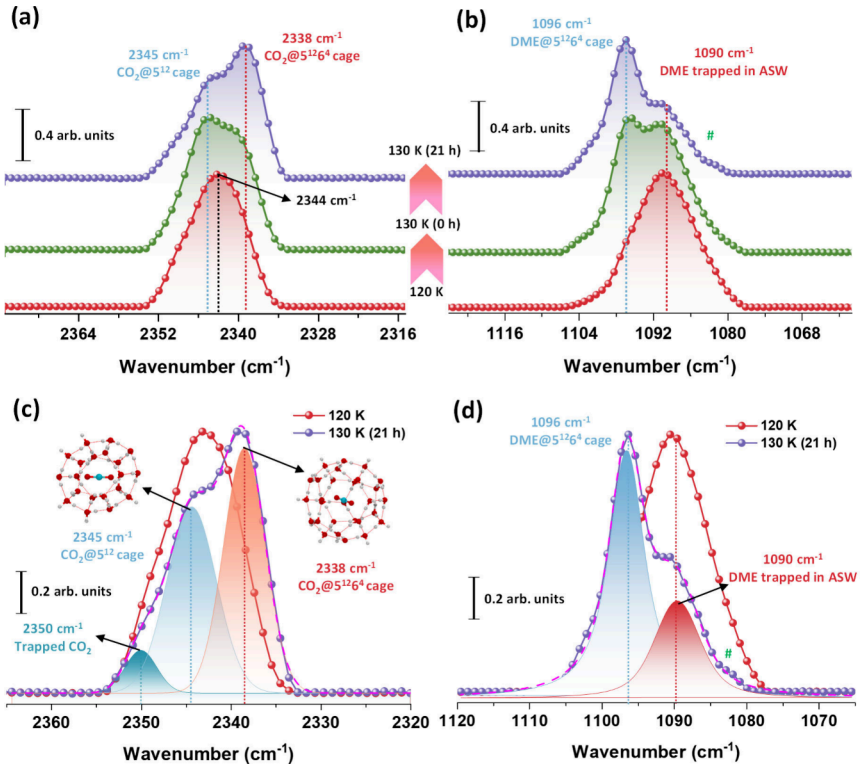

Figure 2. RAIR spectra of CO_2 and DME mixed binary CH. Temperature and time-dependent normalized RAIR spectra of DME (150 ML) @(CO_2+H_2O) (1:10) (150 ML) mixed ice in (a) C=O antisymmetric stretching region for CO_2 and (b) C−O antisymmetric stretching region for DME. A comparison of normalized spectra of same ice in (c) C=O antisymmetric stretching region for CO_2, (d) C−O antisymmetric stretching region for DME at 120 and 130 K (after annealing for 21 h). The spectrum labeled as 130 K (21 h) was deconvoluted to three components, shown in panel c in blue (2345 cm^{-1}), red (2338 cm^{-1}), and cyan blue (2350 cm^{-1}). In panel d, blue (1096 cm^{-1}) and red (1090 cm^{-1}) shades. The peak labeled as # in the spectrum at 130 K and 21 h is attributed to a very tiny amount of DME dilutes. Images depicting CO_2 molecules confined within 5^{12}, $5^{12}6^4$ CH cages and DME molecules within $5^{12}6^4$ CH cages are presented alongside their corresponding peak profiles.

was deposited on Ru(0001) substrate at 10 K. On it, 150 ML of water and CO_2 (10:1, together) were codeposited (illustrated in Figure 1a). The RAIR spectra of CO_2 and DME in the C=O and C−O antisymmetric stretching regions, respectively, are shown in Figure S2. In Figure S2a, the peak at 2346 cm^{-1} corresponds to CO_2 occupying the small cages of the sI clathrate structure, while the peak at 2354 cm^{-1} is due to CO_2 trapped within the pores of amorphous solid water (ASW). The sI CH of CO_2 is typically characterized by Fermi dyad peaks in Raman spectroscopy.[37,38,53−55] However, these features are weakly active in IR spectroscopy due to symmetry-imposed selection rules. Kumar et al.[55] presented a comparative study of sI and sII CO_2 CHs using both Raman and IR spectroscopy. In their work, the Fermi dyad peaks were used for identification in the Raman spectra, while the CO_2 antisymmetric stretch was employed in the IR spectra. Their assignments show good agreement with the present IR data. In Figure S2b, the peak at 1098 cm^{-1} is due to amorphous DME at 10 K. When the system was thermally annealed, DME gradually diffused into the ice matrix, resulting in a mixed system comprising DME, water, and CO_2. This diffusion was accompanied by a red shift in the peak position from 1098 cm^{-1} to 1090 cm^{-1} at 120 K, indicative of hydrogen bonding interactions between water and DME (illustrated in Figure 1b).[25] Here, it is worth noting that both the guest molecules are mobile at this temperature as CO_2 and DME desorb near 90 K, in their pure state in UHV, which is 30 K lower. Continuing the annealing process to 120 K, the peak associated with uncaged CO_2 (2354 cm^{-1}) disappeared completely, while the peak related to caged CO_2 (2344 cm^{-1}) remained, shifting slightly by 2 cm^{-1} from the original position (Figure S2a).

Figure 2a,b shows the normalized RAIR spectra at 120 K, 130 K (0 h), and 130 K (21 h) in the C=O and C−O antisymmetric regions of CO_2 and DME, respectively, in the narrow window of 120−130 K, "while the spectra in the whole temperature range" are given in Figure S2. The peak at 2344 cm^{-1} in the C=O antisymmetric stretching region (Figure 2a) at 120 K is attributed to the CO_2 encaged in small cages of sI CH. In Figure 2b, the peak at 1090 cm^{-1} in C−O antisymmetric region is attributed to the DME trapped in amorphous solid water (ASW), where DME is hydrogen bonded to ASW.[25] Upon further annealing to 130 K, a new peak arose at 2338 cm^{-1}, and the peak at 2344 cm^{-1} got blue-shifted slightly to 2345 cm^{-1}. After 21 h of annealing, the peak at 2338 cm^{-1} exhibited a significant increase in intensity relative to the peak at 2345 cm^{-1}. The new peak at 2338 cm^{-1} can be attributed to large cages of either sI or sII structure, as it does not correspond to any other interaction in pure CO_2 or CO_2−water. Simultaneously, in Figure 2b at 130 K, a new peak arose at 1096 cm^{-1}, which is attributed to DME encaged in the large cages of sII. In our previous study,[25] we extensively discussed the formation of sII CH of DME, wherein DME selectively occupies the large cages. This assignment was supported by both IR spectroscopy and density functional theory calculations. Beyond the well-established cubic sII, Udachin et al. reported that under high-pressure conditions, DME can also occupy three different cage types in a 1:1:1 ratio

https://doi.org/10.1021/acs.jpclett.5c00393
J. Phys. Chem. Lett. 2025, 16, 4982−4989

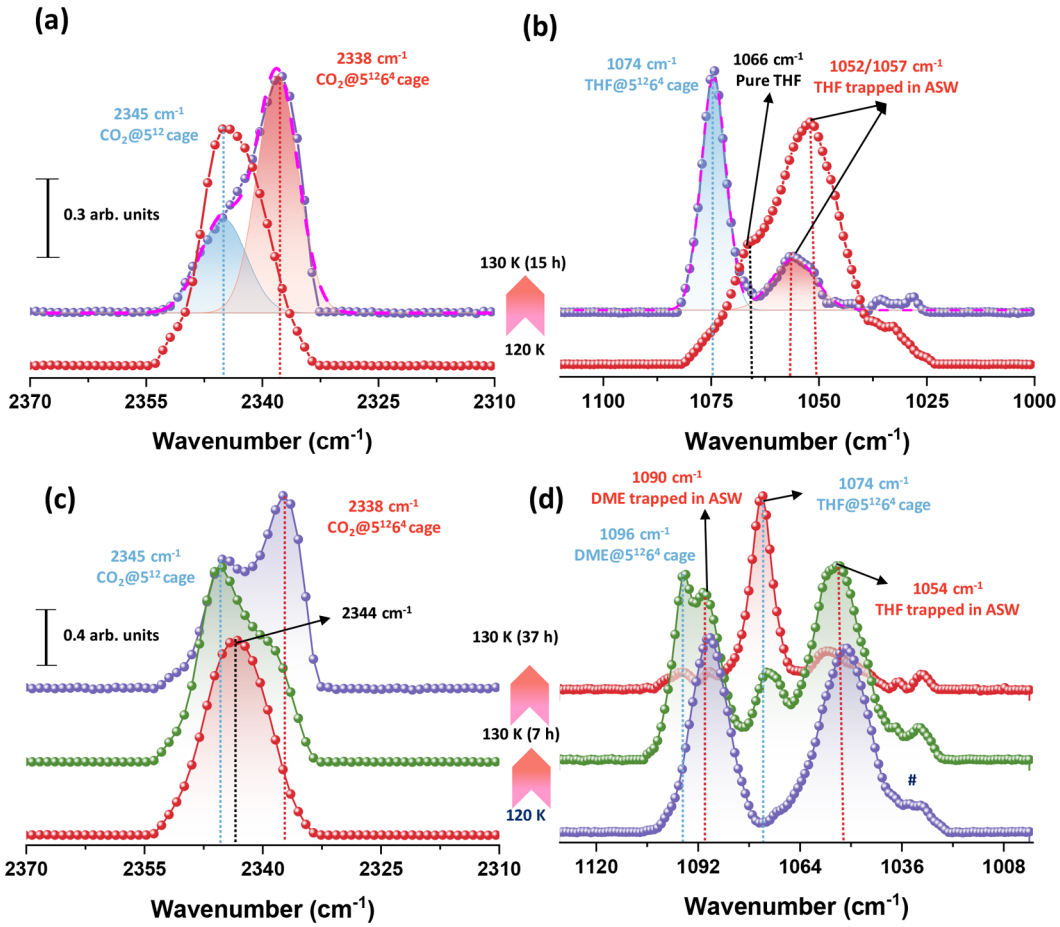

Figure 3. RAIR spectra of the mixed CHs. Temperature- and time-dependent normalized RAIR spectra of THF@(CO_2+H_2O) (50 ML @(20 ML + 180 ML)) mixed ice in (a) C=O antisymmetric stretching region for CO_2, (b) C−O antisymmetric stretching region for THF. Temperature- and time-dependent normalized RAIR spectra of THF@DME@(CO_2+H_2O) (50 ML@50 ML @(20 ML + 180 ML)) mixed ice in (c) C=O antisymmetric stretching region for CO_2 and (d) C−O antisymmetric stretching region for THF and DME.

($5^{12}6^3$:$5^{12}6^2$:$4^2$$5^8$$6^1$), forming a tetragonal clathrate hydrate structure.[56] However, in our current IR measurements, we observed only a single distinct new vibrational feature that is assigned to the occupation of the large cages in the sII hydrate. Further annealing led to the desorption of ASW-trapped DME, with decrease in the 1090 cm^{-1} peak intensity. During this process, the reordering of water molecules occurred, and the RAIR spectra in the O−H stretching region got sharper (Figure S3). Fleyfel et al.[21] demonstrated that the peak at 2338 cm^{-1} corresponded to the large cages of sI CO_2 CH at 135 K in the presence of pure CO_2. However, they also established that when THF was present, CO_2 occupied small cages exclusively while THF occupied large cages of sII CH. Similar findings were reported by Buch et al.[57] in the case where the guest was DME. It is worth noting that in both these studies, CHs were prepared from crystalline ice, whereas in this study, CHs were prepared from an amorphous ice mixture. Additionally, there was no significant shift in the spectrum for the occupancy of large cages of both sI and sII.[58] Our previous research had indicated the instability of the $5^{12}6^2$ cage in the presence of THF molecules in sI CH. Thus, the emergence of the 2338 cm^{-1} peak in the present work is attributed to the large cages of sII CH. We note that although the peak at 2345 cm^{-1} is attributed to the small cages, whether it originates from sI, sII, or both structures cannot be distinguished. In the case of sII clathrate hydrates of DME, where the small cages are empty, CO_2 can also occupy the small cages of the sII structure. Figure 2c,d shows the deconvoluted spectra of CO_2 and DME at 130 K after 21 h, along with the reference spectra at 120 K. It was found that, after 21 h at 130 K, 49% of the CO_2 occupied the newly formed large cages of sII, 45% resided in small cages, and 6% remained trapped in water ice. Similarly, 69% of DME was confined within the large cages of sII, while the remaining 31% was retained in water ice.

To strengthen our claim on the formation of large cages of sII CH of CO_2 and the dynamics of the cages at low temperatures, we used THF as another guest molecule which is known to form stable sII CH. A similar experimental procedure was carried out, where 50 ML of THF was deposited below 250 ML of a CO_2 + water mixture in 1:10 ratio, at 10 K. It was annealed to 130 K and held there for 15 h. At 10 K, THF stayed in an amorphous form (shown in Figure S4), and when annealed to 120 K, a mixed system of CO_2−THF−water was formed. Figure 3a,b shows normalized RAIR spectra of mixed CHs of THF and CO_2 at 120 and 130 K (after 15 h) in the C=O and C−O asymmetric stretching regions, respectively. In Figure 3a, at 120 K, the peak at 2345 cm^{-1} represents CO_2 in small cages of sI, and at 130 K, after 15 h of annealing, the new peak at 2338 cm^{-1} indicates the large cages of sII CH occurs.

https://doi.org/10.1021/acs.jpclett.5c00393
J. Phys. Chem. Lett. 2025, 16, 4982−4989

In Figure 3b, the formation of THF CH is shown. At 120 K, the peak at 1052 cm^{-1} represents the ASW-trapped THF, whereas the peak at 1066 cm^{-1} represents pure amorphous THF. After 15 h at 130 K, a new peak at 1074 cm^{-1} appeared, which showed the formation of large cages of sII hydrate, where THF occupies only the large cages.[42]

Here, the transformation mechanism mirrors that of the DME-CO_2 binary CHs. This transformation of sI to sII CH, where part of the large cages is occupied by CO_2 along with DME/THF, is attributed to better mobility of CO_2 compared to that of DME/THF (in the water matrix) at the annealing temperature. The presence of UHV, and a temperature of 130 K, which is very close to the glass transition temperature (136 K)[59,60] of water ice, creates a favorable environment for the formation, dissociation, and transformation of CHs.[61] At this temperature, most molecules adopt a metastable CH state.[6,25,62] At 130 K, pure CO_2 CH slowly dissociates, and the CO_2 formed is highly mobile compared to DME/THF. In the presence of DME/THF CH, the fraction of molecules coming out from small cages of sI CO_2 CH may nucleate other CHs along with free DME/THF molecules. These free molecules may also participate in the growth of the already nucleated sII hydrate. To explore the importance of intermolecular motion, the prepared DME@CO_2-water ice was kept at 115 K for 25 h where we observed no changes in the C=O stretching region of CO_2 other than a tiny intensity decrease. In the C−O antisymmetric stretching region of DME, a very weak hump was observed at 1096 cm^{-1}, indicating the presence of a minor fraction of sII DME CH (Figure S5). This indicates that no major change occurs in the CO_2 CH when the molecules are not mobile. Our previous study[25,42] showed that DME/THF occupies the large cages of sII CH at 130 K in both the codeposited and sequentially vapor-deposited DME/THF−water ice mixture. So, it is concluded that at 130 K, when DME/THF starts to form sII CH, it breaks the small cage of CO_2 CH and induces the formation of large cages (illustrated in Figure 1c,d). It is worth noting that Figure 1 does not depict the actual physical nucleation process of CHs but rather provides a pictorial representation of the molecules and CH cages.

To study the relative stability of each CH cage in multicomponent CHs, we have taken four-component systems (DME−CO_2−THF−water), created mixed CHs of three guest molecules, and observed the stability of individual CHs in the mixed system. First, 50 ML of THF was deposited on the Ru(0001) substrate, followed by 50 ML of DME, then 200 ML water−CO_2 were codeposited at a 10:1 ratio, at 10 K. Then, the whole system was annealed to 130 K, which created a mixed system of THF−DME−CO_2−water. Then, waiting at the same temperature for 37 h led to the formation, dissociation, desorption, and transformation events simultaneously. Figure 3c,d shows the RAIR spectra of CO_2, DME, and THF in C=O and C−O antisymmetric stretching regions. In Figure 3c, the evolution of CO_2 CH with respect to the temperature and time is shown. At 120 K, the peak at 2344 cm^{-1} represents the CO_2 trapped within 5^{12} cages of sI. Upon annealing at 130 K for 7 h, a new peak emerges at 2338 cm^{-1} (CO_2 trapped in the $5^{12}6^4$ cage). Subsequently, after 42 h, the intensity of the 2338 cm^{-1} peak increases relative to the 2345 cm^{-1} peak. In Figure 3d, the evolution of DME and THF is shown. At 120 K, DME and THF remained in the amorphous form within the ice matrix. After 7 h at 130 K, DME and THF form CH, which is indicated by the increase in the peak intensity at 1096 cm^{-1} and 1074 cm^{-1}, respectively. However, after 37 h, most of the DME desorbs from the matrix, including from the CH cages. This is a very complex system in which all three guest molecules in the same system transform simultaneously. We conclude that THF forms stable crystalline CH inside an amorphous matrix at 130 K,[42] where CO_2 and DME form metastable structures of CH.

We plotted the intensity of the peaks assigned to different molecules encaged in different CH systems versus time in Figure 4 (intensities of different peaks are derived from Figure S6) to better understand the relative stability of CHs. Here, it is worth noting that the assigned peak intensity for each cage is not the individual peak intensity but the overlapped peak intensity with other peaks. These peak intensities can help us understand the relative formation and dissociation of each CH. During thermal annealing for 37 h, the intensity of the peak at 1074 cm^{-1}, representing THF encaged within sII large cages, rises. Concurrently, the intensities of peaks assigned to small (2345 cm^{-1}) and large (2338 cm^{-1}) cages of CO_2 and large cages of DME (1096 cm^{-1}) decrease.

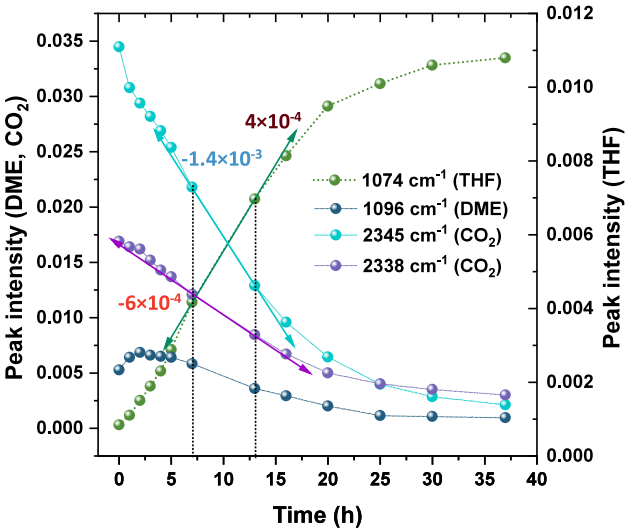

Figure 4. Time-dependent evolution of specific CH in mixed CH at 130 K. Intensity of the peak 1074 cm^{-1} (large cages of THF), 1096 cm^{-1} (large cages of DME), 2345 cm^{-1} (small cage of CO_2), and 2338 cm^{-1} (large cages of CO_2).

During the initial 2 h, increase in the 1096 cm^{-1} peak signifies increase in the formation of DME CH. However, shortly thereafter, it begins to dissociate. Here, the CO_2 transformation is largely dependent on THF, as THF CH is thermodynamically more stable. From the initial time to 20 h, the curves for CO_2 and THF show a linear change. Afterward, we observe saturation in their formation and dissociation. Considering this linear character, we calculated slopes for all three curves between 7 and 13 h; they showed a negative slope for the large cages (6×10^{-4}), less than for the small cages (1.4×10^{-3}), indicating that the fraction of the molecules coming from small cages create large cages, with some of them desorbing from the ice matrix. As we noted earlier, the 2338 cm^{-1} peak is overlapped with the peak at 2346 cm^{-1} and the peak intensity does not directly indicate the percentage of CO_2 in large cages. However, the reduced slope refers to the transformation from small cages to large cages.

https://doi.org/10.1021/acs.jpclett.5c00393
J. Phys. Chem. Lett. 2025, 16, 4982−4989

The nucleation of sII CHs of DME/THF is facile in amorphous ice under UHV conditions at 130 K. At this temperature, all guest molecules exhibit sufficient mobility, as the desorption temperatures of CO_2 and DME are below 100 K, while that of THF is approximately 130 K. Studies report that the glass transition temperature of water lies between 130 and 140 K, enabling water mobility in this range.[59,60,63,64] Previous research showed that metastable CHs dissociated at elevated temperatures, leading to the formation of hexagonal or cubic ice, when the guest molecules have desorption temperatures below 120 K.[3,6,25,62] Additionally, RAIRS studies indicate that nucleation does not occur uniformly across the ice film. The O−H stretching region exhibits partial ordering rather than the sharp, well-defined bands characteristic of fully crystallized ice. Jacobson's theoretical work highlights the importance of amorphous nucleation pathways, favoring intermediate metastable CH formation.[65] Notably, the metastable sII crystal polymorph tends to grow preferentially over the stable sI structure.[66] In this study, all transformations occurred in an amorphous ice environment, promoting the formation of metastable CHs. This environment particularly favors the formation of larger sII cages for CO_2. Overall, the stability and formation of CHs are closely linked to the desorption temperatures of guest molecules, which directly influence their intermolecular motion within the ice matrix. Although this study investigates the formation of large cages of CO_2 clathrate hydrates in the presence of DME, THF, or their mixture under UHV and cryogenic conditions, diffraction studies are necessary to fully resolve the exact structural transitions involved.

In conclusion, we present the first experimental evidence of the formation of large cages of sII CO_2 CH within an amorphous ice matrix in UHV under cryogenic conditions. While CO_2 typically stabilizes within small cages of sI at lower temperatures when it is in the pure form, the introduction of DME and THF promotes the formation of large cages. This phenomenon arises from the facile sII CH formation of DME and THF at 130 K, facilitating the nucleation and occupancy of CO_2 in the large sII cages. The metastable nature of sI CH at this temperature contributes to this intricate process. In the case of mixed CHs, where all three guest molecules are present, prolonged annealing led to an increase in the THF CH fraction over time, resulting in the breaking of most of the large cages of DME and the small cages of CO_2 and the release of DME and CO_2 from the matrix. Interestingly, CO_2 remains in significant quantities within the matrix, predominantly within the larger cages. This study explored the possibility of mixed hydrates in multicomponent interstellar ice mimics, highlighting a dynamic interplay between cages that could influence the evolution of ISM chemistry.

■ ASSOCIATED CONTENT

Supporting Information

The Supporting Information is available free of charge at https://pubs.acs.org/doi/10.1021/acs.jpclett.5c00393.

Experimental section (including experimental setup, materials and reagents, sample preparation) and temperature and time-dependent RAIR spectra (PDF)

Transparent Peer Review report available (PDF)

■ AUTHOR INFORMATION

Corresponding Authors

Rajnish Kumar − *Department of Chemical Engineering, Indian Institute of Technology Madras, Chennai 600036, India; International Centre for Clean Water, IIT Madras Research Park, Chennai 600113, India;* orcid.org/0000-0002-4172-2638; Email: rajnish@iitm.ac.in

Thalappil Pradeep − *DST Unit of Nanoscience (DST UNS) and Thematic Unit of Excellence (TUE), Department of Chemistry, Indian Institute of Technology Madras, Chennai 600036, India; International Centre for Clean Water, IIT Madras Research Park, Chennai 600113, India;* orcid.org/0000-0003-3174-534X; Email: pradeep@iitm.ac.in

Authors

Bijesh K. Malla − *DST Unit of Nanoscience (DST UNS) and Thematic Unit of Excellence (TUE), Department of Chemistry, Indian Institute of Technology Madras, Chennai 600036, India*

Soham Chowdhury − *DST Unit of Nanoscience (DST UNS) and Thematic Unit of Excellence (TUE), Department of Chemistry, Indian Institute of Technology Madras, Chennai 600036, India*

Gaurav Vishwakarma − *DST Unit of Nanoscience (DST UNS) and Thematic Unit of Excellence (TUE), Department of Chemistry, Indian Institute of Technology Madras, Chennai 600036, India;* orcid.org/0009-0002-6076-3299

Complete contact information is available at: https://pubs.acs.org/10.1021/acs.jpclett.5c00393

Author Contributions

T.P. and B.K.M. designed the research. B.K.M. and S.C. have performed the experiments. T.P. and R.K. supervised its progress. B.K.M. analyzed the results. The first draft of the manuscript was written by B.K.M. The final version of the manuscript was prepared, including the contributions of all authors.

Notes

The authors declare no competing financial interest.

■ ACKNOWLEDGMENTS

We acknowledge the Science and Engineering Research Board (SERB), Department of Science and Technology (DST), and Government of India for research funding. T.P. acknowledges funding from the Centre of Excellence on Molecular Materials and Functions under the Institution of Eminence scheme of IIT Madras. B.K.M. thanks the Council of Scientific and Industrial Research (CSIR) for his research fellowship. G.V. and S.C. thank IITM for their research fellowship. T.P. acknowledges funding from a JC Bose Fellowship.

■ REFERENCES

(1) Tychengulova, A.; Katpayeva, K.; Shomshekova, S.; Ibragimova, S.; Golikov, O.; Yerezhep, D.; Sokolov, D.; Aldiyarov, A. Laboratory Studies of the Clathrate Hydrate Formation in the Carbon Dioxide-Water Mixtures at Interstellar Conditions. *ACS Omega* **2025**, *10* (1), 1237−1248.

(2) Ghosh, J.; Methikkalam, R. R. J.; Bhuin, R. G.; Ragupathy, G.; Choudhary, N.; Kumar, R.; Pradeep, T. Clathrate Hydrates in Interstellar Environment. *Proc. Natl. Acad. Sci. U. S. A.* **2019**, *116* (5), 1526−1531.

(3) Ghosh, J.; Vishwakarma, G.; Kumar, R.; Pradeep, T. Formation and Transformation of Clathrate Hydrates under Interstellar Conditions. *Acc. Chem. Res.* **2023**, *56* (16), 2241−2252.
(4) Ghosh, J.; Bhuin, R. G.; Vishwakarma, G.; Pradeep, T. Formation of Cubic Ice via Clathrate Hydrate, Prepared in Ultrahigh Vacuum under Cryogenic Conditions. *J. Phys. Chem. Lett.* **2020**, *11* (1), 26−32.
(5) Malla, B. K.; Vishwakarma, G.; Chowdhury, S.; Selvarajan, P.; Pradeep, T. Formation of Ethane Clathrate Hydrate in Ultrahigh Vacuum by Thermal Annealing. *J. Phys. Chem. C* **2022**, *126* (42), 17983−17989.
(6) Vishwakarma, G.; Malla, B. K.; Chowdhury, S.; Khandare, S. P.; Pradeep, T. Existence of Acetaldehyde Clathrate Hydrate and Its Dissociation Leading to Cubic Ice under Ultrahigh Vacuum and Cryogenic Conditions. *J. Phys. Chem. Lett.* **2023**, *14* (23), 5328−5334.
(7) Malla, B. K.; Yang, D.-S.; Pradeep, T. Growth of Clathrate Hydrates in Nanoscale Ice Films Observed Using Electron Diffraction and Infrared Spectroscopy. *J. Phys. Chem. Lett.* **2025**, *16* (1), 365−371.
(8) Sloan, E. D., Jr.; Koh, C. A.; Koh, C. A. *Clathrate Hydrates of Natural Gases*; CRC Press, 2007.
(9) Takeya, S.; Shimada, W.; Kamata, Y.; Ebinuma, T.; Uchida, T.; Nagao, J.; Narita, H. In Situ X-Ray Diffraction Measurements of the Self-Preservation Effect of CH4 Hydrate. *J. Phys. Chem. A* **2001**, *105* (42), 9756−9759.
(10) Yamamoto, K.; Misawa, T.; Ito, H.; Takeya, S.; Alavi, S.; Ohmura, R. Phase Equilibrium Conditions and Crystal Structure of Binary Hydrates Formed with 1-Methylpiperidine. *J. Phys. Chem. C* **2024**, *128* (3), 1312−1322.
(11) Ratcliffe, C. I. The Development of Clathrate Hydrate Science. *Energy Fuels* **2022**, *36* (18), 10412−10429.
(12) Thakre, N.; Jana, A. K. Physical and Molecular Insights to Clathrate Hydrate Thermodynamics. *Renew. Sustain. Energy Rev.* **2021**, *135*, 110150.
(13) Sloan, E. D. J.; Koh, C. A. Introduction: Clathrate Hydrates of Natural Gases. *Clathrate Hydrates Nat. Gases* **2008**, I−XXV.
(14) Davy, H., VIII On a Combination of Oxymuriatic Gas and Oxygene Gas. *Philos. Trans. R. Soc. London* **1811**, *101*, 155−162.
(15) Blake, D.; Allamandola, L.; Sandford, S.; Hudgins, D.; Freund, F. Clathrate Hydrate Formation in Amorphous Cometary Ice Analogs in Vacuo. *Science.* **1991**, *254* (5031), 548−551.
(16) Fleyfel, F.; Devlin, J. P. Infrared Spectra of Large Clusters Containing Small Ether Molecules: Liquid, Crystalline, and Clathrate-Hydrate Cluster Spectra. *J. Chem. Phys.* **1990**, *92* (1), 36−42.
(17) Fleyfel, F.; Devlin, J. P. FT-IR Spectra of 90 K Films of Simple, Mixed, and Double Clathrate Hydrates of Trimethylene Oxide, Methyl Chloride, Carbon Dioxide, Tetrahydrofuran, and Ethylene Oxide Containing Decoupled D2O. *J. Phys. Chem.* **1988**, *92* (3), 631−635.
(18) Williams, K. D.; Devlin, J. P. Formation and Spectra of Clathrate Hydrates of Methanol and Methanol-Ether Mixtures. *J. Mol. Struct.* **1997**, *416* (1−3), 277−286.
(19) Ritzhaupt, G.; Devlin, J. P. Infrared Spectra of Nitric and Hydrochloric Acid Hydrate Thin Films. *J. Phys. Chem.* **1991**, *95*, 90−95.
(20) Bertie, J. E.; Devlin, J. P. Infrared Spectroscopic Proof of the Formation of the Structure I Hydrate of Oxirane from Annealed Low-Temperature Condensate. *J. Chem. Phys.* **1983**, *78* (10), 6340−6341.
(21) Fleyfel, F.; Devlin, J. P. Carbon Dioxide Clathrate Hydrate Epitaxial Growth: Spectroscopic Evidence for Formation of the Simple Type-II CO2 Hydrate. *J. Phys. Chem.* **1991**, *95* (9), 3811−3815.
(22) Choukroun, M.; Vu, T. H.; Fayolle, E. C. No Compelling Evidence for Clathrate Hydrate Formation under Interstellar Medium Conditions over Laboratory Time Scales. *Proc. Natl. Acad. Sci. U. S. A.* **2019**, *116* (29), 14407−14408.
(23) Ghosh, J.; Methikkalam, R. R. J.; Bhuin, R. G.; Ragupathy, G.; Choudhary, N.; Kumar, R.; Pradeep, T. Reply to Choukroun et Al.: IR and TPD Data Suggest the Formation of Clathrate Hydrates in Laboratory Experiments Simulating ISM. *Proc. Natl. Acad. Sci. U. S. A.* **2019**, *116* (29), 14409−14410.
(24) Vishwakarma, G.; Malla, B. K.; Reddy, K. S. S. V. P.; Ghosh, J.; Chowdhury, S.; Yamijala, S. S. R. K. C.; Reddy, S. K.; Kumar, R.; Pradeep, T. Induced Migration of CO 2 from Hydrate Cages to Amorphous Solid Water under Ultrahigh Vacuum and Cryogenic Conditions. *J. Phys. Chem. Lett.* **2023**, *14* (11), 2823−2829.
(25) Malla, B. K.; Vishwakarma, G.; Chowdhury, S.; Nayak, S. K.; Yamijala, S. S. R. K. C.; Pradeep, T. Formation and Dissociation of Dimethyl Ether Clathrate Hydrate in Interstellar Ice Mimics. *J. Phys. Chem. C* **2024**, *128* (6), 2463−2470.
(26) Arumainayagam, C. R.; Garrod, R. T.; Boyer, M. C.; Hay, A. K.; Bao, S. T.; Campbell, J. S.; Wang, J.; Nowak, C. M.; Arumainayagam, M. R.; Hodge, P. J. Extraterrestrial Prebiotic Molecules: Photochemistry vs. Radiation Chemistry of Interstellar Ices. *Chem. Soc. Rev.* **2019**, *48* (8), 2293−2314.
(27) Luspay-Kuti, A.; Mousis, O.; Hässig, M.; Fuselier, S. A.; Lunine, J. I.; Marty, B.; Mandt, K. E.; Wurz, P.; Rubin, M. The Presence of Clathrates in Comet 67P/Churyumov-Gerasimenko. *Sci. Adv.* **2016**, *2* (4), No. e1501781.
(28) Takeya, S.; Fujihisa, H.; Alavi, S.; Ohmura, R. Thermally Induced Phase Transition of Cubic Structure II Hydrate: Crystal Structures of Tetrahydropyran-CO2 Binary Hydrate. *J. Phys. Chem. Lett.* **2023**, *14* (7), 1885−1891.
(29) Takeya, S.; Udachin, K. A.; Moudrakovski, I. L.; Susilo, R.; Ripmeester, J. A. Direct Space Methods for Powder X-Ray Diffraction for Guest-Host Materials: Applications to Cage Occupancies and Guest Distributions in Clathrate Hydrates. *J. Am. Chem. Soc.* **2010**, *132* (2), 524−531.
(30) Muromachi, S.; Takeya, S.; Alavi, S.; Ripmeester, J. A. Structural CO 2 Capture Preference of Semiclathrate Hydrate Formed with Tetra- n -Butylammonium Chloride. *CrystEngComm* **2022**, *24* (24), 4366−4371.
(31) Misawa, T.; Ishikawa, T.; Takeya, S.; Alavi, S.; Ohmura, R. Continuous Hydrate-Based CO2 Separation from H2 + CO2 Gas Mixture Using Cyclopentane as Co-Guest. *J. Ind. Eng. Chem.* **2023**, *121*, 228−234.
(32) Maruyama, M.; Takeya, S.; Yoneyama, A.; Ishikawa, T.; Misawa, T.; Nagayama, S.; Alavi, S.; Ohmura, R. Characterization of Clathrate Hydrates with CO2 + 1-Propanol or 2-Propanol: Implications for Flow Assurance, Refrigeration, Carbon Capture, and Skincare Applications. *J. Ind. Eng. Chem.* **2024**, *131*, 305−314.
(33) Sun, D.; Daraboina, N.; Ripmeester, J.; Englezos, P. Capture of CO_2 and Storage in Depleted Gas Reservoirs in Alberta as Gas Hydrate. In *Gas Injection for Disposal and Enhanced Recovery*; Wiley, 2014; Vol. *9781118938*, pp 305−310.
(34) Dadhich, R.; Babu, P.; Daraboina, N. Kinetic and Performance Assessment of Hydrate-Based Precombustion CO 2 Capture Using Dry Water. *Energy & Fuels.* **2024**, *38* (24), 23625−23632.
(35) Bauer, R. P. C.; Ravichandran, A.; Tse, J. S.; Appathurai, N.; King, G.; Moreno, B.; Desgreniers, S.; Sammynaiken, R. In Situ X-Ray Diffraction Study on Hydrate Formation at Low Temperature in a High Vacuum. *J. Phys. Chem. C* **2021**, *125* (48), 26892−26900.
(36) Babu, P.; Linga, P.; Kumar, R.; Englezos, P. A Review of the Hydrate Based Gas Separation (HBGS) Process for Carbon Dioxide Pre-Combustion Capture. *Energy* **2015**, *85*, 261−279.
(37) Chen, L.; Lu, H.; Ripmeester, J. A. Raman Spectroscopic Study of CO2 in Hydrate Cages. *Chem. Eng. Sci.* **2015**, *138*, 706−711.
(38) Yao, Y.; Yin, Z.; Kumar, R.; Gao, X.; Chen, D. Tuning Effect of DIOX on the Thermodynamics and Cage Occupancy of CH4/CO2 + DIOX Mixed Hydrates. *Chem. Eng. J.* **2024**, *482*, 148984.
(39) Yao, Y.; Yin, Z.; Niu, M.; Liu, X.; Zhang, J.; Chen, D. Evaluation of 1,3-Dioxolane in Promoting CO2 Hydrate Kinetics and Its Significance in Hydrate-Based CO2 Sequestration. *Chem. Eng. J.* **2023**, *451*, 138799.
(40) Boese, A. D.; Boese, R. Tetrahydrothiophene and Tetrahydrofuran, Computational and x-Ray Studies in the Crystalline Phase. *Cryst. Growth Des.* **2015**, *15* (3), 1073−1081.

https://doi.org/10.1021/acs.jpclett.5c00393
J. Phys. Chem. Lett. 2025, 16, 4982−4989

(41) Sargent, D. F.; Calvert, L. D. Crystallographic Data for Some New Type II Clathrate Hydrates. *J. Phys. Chem.* **1966**, *70* (8), 2689−2691.
(42) Ghosh, J.; Bhuin, R. G.; Ragupathy, G.; Pradeep, T. Spontaneous Formation of Tetrahydrofuran Hydrate in Ultrahigh Vacuum. *J. Phys. Chem. C* **2019**, *123* (26), 16300−16307.
(43) Gough, S. R.; Garg, S. K.; Ripmeester, J. A.; Davidson, D. W. Dielectric Relaxation and Nuclear Magnetic Resonance Studies of Two Clathrate Hydrates of Dimethyl Ether. *J. Phys. Chem.* **1977**, *81* (23), 2158−2163.
(44) D'Hendecourt, L. B.; Jourdain de Muizon, M.; D'Hendecourt, L. B.; Jourdain de Muizon, M. The Discovery of Interstellar Carbon Dioxide. *A&A* **1989**, *223*, L5−L8.
(45) Snyder, L. E.; Buhl, D.; Schwartz, P. R.; Clark, F. O.; Johnson, D. R.; Lovas, F. J.; Giguere, P. T. Radio Detection of Interstellar Dimethyl Ether. *Astrophys. J.* **1974**, *191*, L79.
(46) McGuire, B. A.; Carroll, P. B.; Loomis, R. A.; Finneran, I. A.; Jewell, P. R.; Remijan, A. J.; Blake, G. A. Discovery of the Interstellar Chiral Molecule Propylene Oxide (CH3CHCH2O). *Science.* **2016**, *352* (6292), 1449−1452.
(47) McGuire, B. A.; Carroll, P. B.; Loomis, R. A.; Finneran, I. A.; Jewell, P. R.; Remijan, A. J.; Blake, G. A. Detection of Interstellar Ethylene Oxide (c-C2H4O). *Science (80-.).* **2016**, *352* (6292), 1449−1452.
(48) Bag, S.; Bhuin, R. G.; Methikkalam, R. R. J.; Pradeep, T.; Kephart, L.; Walker, J.; Kuchta, K.; Martin, D.; Wei, J. Development of Ultralow Energy (1−10 EV) Ion Scattering Spectrometry Coupled with Reflection Absorption Infrared Spectroscopy and Temperature Programmed Desorption for the Investigation of Molecular Solids. *Rev. Sci. Instrum.* **2014**, *85* (1), 014103.
(49) Malla, B. K.; Vishwakarma, G.; Chowdhury, S.; Pradeep, T. Vacuum Ultraviolet Photolysis of Condensed Methyl Chloride in Interstellar Model Conditions and Trapping of Intermediates at Intergrain Interfaces. *J. Phys. Chem. C* **2023**, *127* (50), 24149−24157.
(50) Escribano, R. M.; Muñoz Caro, G. M.; Cruz-Diaz, G. A.; Rodríguez-Lazcano, Y.; Maté, B. Crystallization of CO 2 Ice and the Absence of Amorphous CO 2 Ice in Space. *Proc. Natl. Acad. Sci. U. S. A.* **2013**, *110* (32), 12899−12904.
(51) Edridge, J. L.; Freimann, K.; Burke, D. J.; Brown, W. A. Surface Science Investigations of the Role of CO 2 in Astrophysical Ices. *Philos. Trans. R. Soc. A Math. Phys. Eng. Sci.* **2013**, *371* (1994), 20110578.
(52) Hernandez, J.; Uras, N.; Devlin, J. P. Coated Ice Nanocrystals from Water-Adsorbate Vapor Mixtures: Formation of Ether - CO2 Clathrate Hydrate Nanocrystals at 120 K. *J. Phys. Chem. B* **1998**, *102* (23), 4526−4535.
(53) Zhou, X.; Zhou, J.; Chen, P.; Wen, H.; Zang, X.; Fan, S.; Liang, D. Spectral Analysis on the Raman Peaks of CH4, CO2, and N2 in the Hydrate Phase. *Energy Fuels* **2025**, *39* (3), 1579−1587.
(54) Jeenmuang, K.; Pornaroontham, P.; Fahed Qureshi, M.; Linga, P.; Rangsunvigit, P. Micro Kinetic Analysis of the CO2 Hydrate Formation and Dissociation with L-Tryptophan in Brine via High Pressure in Situ Raman Spectroscopy for CO2 Sequestration. *Chem. Eng. J.* **2024**, *479*, 147691.
(55) Kumar, R.; Lang, S.; Englezos, P.; Ripmeester, J. Application of the ATR-IR Spectroscopic Technique to the Characterization of Hydrates Formed by CO2, CO2/H2 and CO 2/H2/C3H8. *J. Phys. Chem. A* **2009**, *113* (22), 6308−6313.
(56) Udachin, K. A.; Ratcliffe, C. I.; Ripmeester, J. A. A Dense and Efficient Clathrate Hydrate Structure with Unusual Cages. *Angew. Chemie Int. Ed.* **2001**, *40* (7), 1303−1305.
(57) Buch, V.; Devlin, J. P.; Monreal, I. A.; Jagoda-Cwiklik, B.; Uras-Aytemiz, N.; Cwiklik, L. Clathrate Hydrates with Hydrogen-Bonding Guests. *Phys. Chem. Chem. Phys.* **2009**, *11* (44), 10245−10265.
(58) Truong-Lam, H. S.; Truong-Lam, H. S.; Seo, S. D.; Kim, S.; Seo, Y.; Lee, J. D. In Situ Raman Study of the Formation and Dissociation Kinetics of Methane and Methane/Propane Hydrates. *Energy Fuels* **2020**, *34* (5), 6288−6297.
(59) Kohl, I.; Bachmann, L.; Mayer, E.; Hallbrucker, A.; Loerting, T. Glass Transition in Hyperquenched Water? *Nat. 2005 4357041* **2005**, *435* (7041), No. E1.
(60) Souda, R. Glass Transition and Intermixing of Amorphous Water and Methanol. *Phys. Rev. Lett.* **2004**, *93* (23), 1−4.
(61) Gudipati, M. S.; Fleury, B.; Wagner, R.; Henderson, B. L.; Altwegg, K.; Rubin, M. Thermal Behavior of Astrophysical Amorphous Molecular Ices. *Faraday Discuss.* **2023**, *245* (0), 467−487.
(62) Ghosh, J.; Vishwakarma, G.; Das, S.; Pradeep, T. Facile Crystallization of Ice I h via Formaldehyde Hydrate in Ultrahigh Vacuum under Cryogenic Conditions. *J. Phys. Chem. C* **2021**, *125* (8), 4532−4539.
(63) Chonde, M.; Brindza, M.; Sadtchenko, V. Glass Transition in Pure and Doped Amorphous Solid Water: An Ultrafast Microcalorimetry Study. *J. Chem. Phys.* **2006**, *125* (9), 94501.
(64) Tsekouras, A. A.; Iedema, M. J.; Cowin, J. P. Amorphous Water-Ice Relaxations Measured with Soft-Landed Ions. *Phys. Rev. Lett.* **1998**, *80* (26), 5798−5801.
(65) Jacobson, L. C.; Hujo, W.; Molinero, V. Amorphous Precursors in the Nucleation of Clathrate Hydrates. *J. Am. Chem. Soc.* **2010**, *132* (33), 11806−11811.
(66) Jacobson, L. C.; Molinero, V. Can Amorphous Nuclei Grow Crystalline Clathrates? The Size and Crystallinity of Critical Clathrate Nuclei. *J. Am. Chem. Soc.* **2011**, *133* (16), 6458−6463.

https://doi.org/10.1021/acs.jpclett.5c00393
J. Phys. Chem. Lett. 2025, 16, 4982−4989